A mechanism for chromite growth in ophiolite complexes: evidence from 3D high-resolution X-ray computed tomography images of chromite grains in Harold's Grave chromitite in the Shetland ophiolite.

Hazel M. Prichard[a] , Stephen J. Barnes[b*] and Belinda Godel[b].

a School of Earth and Ocean Sciences, Cardiff University, Cardiff, CF10 3AT, Wales, UK.

b CSIRO Mineral Resources, Kensington, WA, 6151, Australia.

*Steve.barnes@csiro.au corresponding author

Deceased Jan 2017.

Keywords: Podiform chromite, high resolution X-ray computed tomography, Shetland, ophiolite.

Abstract

A fundamental difference exists between the textures of chromite crystals in chromitites in layered complexes and ophiolites. Those in layered complexes generally have euhedral octahedral shapes except where sintered, whereas those in ophiolites generally have rounded shapes accompanied commonly by nodular and more rarely dendritic chromite. Here we describe another texture characteristic of ophiolitic chromitite. The analysis of high resolution X-ray computed tomography images of chromitite from Harold's Grave in the Shetland ophiolite has revealed 3D hopper structures on chromite grains. In 2D, these hopper structures appear at the surface of the chromite grain as stepped inward facing edges. A study of chromitites in 2D from ten ophiolite complexes has shown that all commonly contain chromite grains displaying these stepped edges. They occur mainly in protected enclaves surrounded by chromite grains that otherwise have rounded edges. The hopper crystals and the often associated clusters of inclusions represent periods of chromite crystal growth in a chromite supersaturated magma due to the presence of a more supercooled and more volatile-rich magma than that present in most layered complexes. Subsequent exposure of chromite crystals to chromite-undersaturated magma caused corrosion, resulting in the characteristic rounded shape of the ophiolitic chromite grains.

Introduction

The crystallisation of rocks largely composed of chromite remains one of the long standing puzzles in igneous petrology. Chromium, a major component of chromite, is typically present in mafic magmas at concentrations of a few hundred ppm at chromite saturation (Barnes, 1986; Murck and Campbell, 1986; Campbell and Murck, 1993), such that chromite growth requires a very large volume of magma relative to the volume of chromite produced. Furthermore, cubic chromite shows a surprisingly wide range of crystal morphologies. Chromite grains in ophiolites are commonly rounded, which has led to suggestions of chemical resorption or mechanical abrasion (e.g. Leblanc and Ceuleneer, 1992). Dendritic grains suggestive of rapid growth from supersaturated magmas are known from ophiolites (e.g. Prichard et al., 2015) and a variety of other settings e.g. komatiites (Godel et al., 2013) and magmatic sulfide-silicate contacts (Dowling et al., 2004; Barnes et al., 2016). Lobate, inclusion-rich "amoeboidal" grains from the Bushveld layered intrusion have been interpreted as modification of dendritic grains (Vukmanovic et al., 2013). Here we report new observations on a well-studied ophiolitic chromitite locality (the Harold's Grave chromitite in the Shetland ophiolite), elucidating the growth mechanism of what initially appear to be typical rounded grains. We argue that these observations provide new insight into the crystallisation of ophiolitic chromitites in particular and igneous cumulates in general.

Ophiolitic chromitite

Most chromitites occur in layered intrusions, such as the Bushveld Complex, or in ophiolite complexes. Ophiolites are fossilised fragments of oceanic lithosphere containing podiform chromitite present in mantle or overlying crustal ultramafic lithologies. In the mantle they form lenses or pods usually surrounded by an envelope of dunite in depleted harzburgite. In the overlying crustal sequence the chromitite has a more stratiform appearance forming discontinuous layers, usually surrounded by dunite (e.g. Peters, 1974; Brown, 1980; Brough et al., 2015; Ceuleneer and Nicolas, 1985; Roberts and Neary, 1993; Melcher et al., 1997; Pagé and Barnes, 2009).
There are marked differences in chromite morphology between layered complexes and ophiolites (Fig. 1). Layered intrusion chromites tend to be form either euhedral octahedra or sintered adcumulate aggregates with curved interfacial boundaries and 120 degree triple points (Hulbert and Von Gruenewaldt, 1985; Godel, 2015). Where textures are not obscured by the sintering or by the widespread (mostly brittle) deformation characteristic of ophiolites, chromites are rounded subhedral to anhedral (e.g. Brown, 1980; Thayer, 1980; Yang and Seccombe, 1993; Zhou et al., 1996; Leblanc, 1980). Maximum sizes for ophiolitic chromitite grains tend to be 1-3 cm (Prichard and Neary, 1981; McElduff and Stumpfl, 1991; Zhou et al., 1996; Melcher et al., 1997), generally larger than the sub-mm grain sizes characteristic of chromitites in layered intrusions (e.g. O'Driscoll et al., 2010; Barnes and Jones, 2012).

Harold's Grave chromite

We investigated chromitites at the Harold's Grave locality in the Shetland ophiolite complex, located in the Shetland Islands, NE of the Scottish mainland, UK (Flinn, 1985; Prichard, 1985; Brough et al., 2015). These chromitites display many of the characteristics of those described above for ophiolitic chromitite. They form one of a number of podiform chromitites surrounded by dunite lenses within tectonised mantle harzburgite (Fig. 2). The Shetland ophiolite is thought to have formed in a supra-subduction zone setting. The dykes at the top of the gabbro show evidence for both MORB and boninitic magmas (Prichard and Lord, 1988). Further evidence for diverse source magmas comes from petrogenetic studies of the various chromitite pods within the Baltasound area (O'Driscoll et al', 2012; Derbyshire et al., 2013). These studies highlight significant short-range variability in chemical and Os isotopic characteristics, implying derivation from a source with short-range heterogeneity feeding magmas through a series of distinct conduits. The Harold's Grave chromitite is distinct from the other chromitites in the ophiolite having lower Mg#, a lower Fe^{3+}/Fe^{2+} ratio and elevated concentrations of TiO_2, V_2O_5, Zn, suggesting formation from a reduced magma (Brough et al., 2015). The Harold's Grave chromite is notably enriched in Ir, Ru, Os and Rh, containing values of 10s of µg/g total PGEs (Prichard and Lord, 1988). Minor magnetite alteration is observed along fractures in the Harold's Grave chromitites, but typically not along grain boundaries. While the chromite grains commonly show pull-apart textures due to volume expansion of the rock mass during serpentinization, original grain boundaries appear to be well preserved.

Methodology and material

X-ray computed tomography (XCT) is a non-destructive technique, originally developed as a medical imaging technique (Hounsfield, 1973), that allows the exploration of the 3-dimensional (3D) characteristics of solid material. Over the past decade or so, XCT has successfully been used to unlock some of the most fundamental challenge in igneous petrology by providing new insight into familiar rock textures when viewed using conventional microscopy on polished thin section in 2D (Barnes, et al., 2008; Godel, et al., 2006; Godel, 2013; Jerram et al., 2010; Ketcham and Carlson, 2001; Philpotts and Dickson, 2000). Recent development in high-resolution XCT (HRXCT) allows the acquisition of data across a range of scale (from mm down to 100's of nm) on specimen rock across and range of mineral densities and has notably been used to characterize the 3D morphology of chromite in various settings (Godel, et al. 2013; Prichard et al., 2015; Vukmanovic, et al, 2013). The combination of HRXCT with the development of processing workflows, algorithms and software is opening a new area aiming at quantifying accurately 3D textures.

A core of 4 mm diameter and 5 mm length was drilled through a sample of chromitite from Harold's Grave (sample HG6A, described in Brough et al. (2015)) in order to image in detail the 3D characteristics of the "hopper" crystal. The core was scanned twice using the XRADIA (now Zeiss) XRM 500 high-resolution 3D X-ray microscope installed at the Australian Resources Research Centre (CSIRO Mineral Resources, Kensington, Western Australia). The entire core was scanned at 2.1 µm voxel size (data not presented) to select a volume of interest (VOI) within the core to highlight details of chromite grain morphology. This VOI was scan at higher resolution (700 nm voxel size). The scanner was set-up to maximise the contrast between the different phases of interests (namely chromite, various silicates and platinum-group minerals) and reduce potential artefacts. The scanner was tuned to a voltage of 140 kV, a power of 10 W and a current of 60 mA. A physical filter (glass doped with metal) was placed in front of the x-ray source to improve signal and reduce beam hardening effect, 3000 projections of the specimen were recorded over 360^{o} (i.e. one projection per 0.12 degree rotation) and were used to reconstruct the 3D volume. Ring artefacts were minimized during acquisition using dynamic ring removal processing and monitored during volume reconstruction (no ring artefact was observed on the dataset, Fig. 3). No beam hardening was observed in the reconstructed dataset (Fig. 3) and hence no correction for beam hardening was made. The 3D volume was processed and analysed using the image processing workflow described in Godel, 2013. A non-local mean filter (Buades et al., 2010) was applied to reduce noise and facilitate image segmentation. It should be noted that this type of filter is edge preserving and hence does not affect surface morphology. A modified version of the 3D-gradient watershed segmentation algorithm presented in Godel (2013) was used to segment the data into 3 different phases (chromite, silicates and platinum-group mineral). This algorithm originally developed to quantify the size and texture of platinum-group mineral in igneous rock (Godel, et al. 2010) permits attribution of a range of greyscales to a particular mineral phase based on its textural relationship (an optimal value is calculated for each voxel by taking into account gradient boundary across mineral species of variable densities). After segmentation, the resulting binary images were rendered in 3D to highlight the 3D morphology of chromite crystals and the silicate inclusions.

Reflected light petrography was carried out on chromitites from Harold's Grave and other pods in the Shetland ophiolite, and from nine more ophiolite complexes: Leka, Norway (Pedersen et al., 1993), Kempersai, Kazakhstan (Melcher et al., 1997), Troodos, Cyprus (McElduff and Stumpfl, 1991), Semail, UAE and Oman (Brown, 1980), Al 'Ays, Saudi Arabia (Prichard et al., 2008a), Pindos, Greece (Prichard et al., 2008b), Berit, Turkey (Kozul et al., 2014), Bragança, Portugal (Bridges et al., 1995) and Santa Elena, Costa Rica (Prichard et al., 1989).

Results

High-resolution X-ray computed tomography was used to determine the morphology of chromite crystal observed in chromitite from Harold's Grave, allowing the recognition of a "hopper" chromite crystal displaying distinctive stepped crystal faces (Figs. 3 and 4). This observation prompted led us to re-examine chromite grain boundary textures from a number of other localities using conventional optical petrography. The term "hopper crystal" is a widely used morphological term denoting a particular kind of dendritic crystal form where the edges of a grain are fully developed but the interior spaces are not filled in (Fig. 5). (The reference is related to the cross-sectional shaped of hopper wagons used to transport grain). This feature results from uneven crystal growth under disequilibrium conditions whereby crystal faces grow faster at their edges than in their centres.

Chromite crystal shapes in 3D

The presence of euhedral planar crystal faces covering the surface of the chromite grains in sample HG6A was revealed after image reconstruction, processing and 3D rendering (Fig. 3 and 4). On one chromite crystal face, the flat surfaces are arranged in steps that form a depression in the centre surrounded by elevated faces; this morphology is characteristic of a partially formed hopper crystal (Fig. 4). Observation in 3D confirms that this surface is not one side of a jigsaw-fit (pull-apart) fracture (Fig. 4D), but preserves the original growth facets uninhibited by impingement on neighbouring crystals. The grains also contain many euhedral equant rectangular or cubic silicate inclusions (negative crystals) that are oriented in rows parallel to the surface of the chromite (Fig 6). This is observed in 3D in a way that would not be possible in 2D. A perfectly formed hopper crystal (Fig. 5) has cross sections marked to illustrate what would be observed in 2D.

Textures observed in 2D

The most easily recognisable hopper faces observed on a 2D polished thin section appear as stepped depressions on the edge of the chromite with the steps facing inwards towards each other, at scales from 50 microns to 0.5 mm. Examination of chromitites from ten different ophiolites including Shetland (Table 1) led to the recognition of stepped edges on chromites in all of them. These stepped edges are interpreted as 2D intersections through hopper crystal faces. (Fig . 7).

Negative crystals and silicate inclusions

Inclusions in chromite grains are more abundant in some samples than others, and indeed in some grains more than others; in some cases (e.g. Fig. 6) individual grains have sieve-like textures with large numbers of inclusions while surrounding grains contain hardly any. The 3D image of the chromite grains from Harold's Grave show that equant cubic negative crystal inclusions occur in rows parallel to the surface of the chromite grain. In 2D inclusions sometimes appear to be an extension of the hopper crystal into the interior of the chromite grain (e.g. Fig. 7 I and M). Inclusion-bearing grains commonly show stepped hopper edges.

Discussion

Hopper formation and initial chromite crystal growth

The combination of 2D and 3D images presented here indicates that stepped, hopper grain boundaries are widespread in ophiolitic chromite grains and are revealing of the growth mechanisms of chromite crystals. Hopper textures form part of the continuum of morphologies from euhedral to dendritic crystal morphologies. This continuum reflects different rates of diffusion-limited crystal growth. Hopper crystals form where the growth mechanism begins to be controlled by differential growth rates at the edges of particular facets; fast growing facets grow out, and are bounded by slower growing ones. As growth rate increases relative to the diffusion rate of essential nutrients through the solute, in this case Cr through the magma, depleted boundary layers begin to develop around the growing crystal. Those faces that are closest to the edge of the boundary layer, or that project through it, continue to grow, while those furthest from undepleted fresh solute are starved and stop growing. As this effect becomes more extreme, dendritic textures develop and form where crystals grow from strongly supersaturated liquids. Delay in nucleation results in very rapid growth from sparsely distributed nuclei, giving rise to extreme dendritic morphologies such as harrisites in layered intrusions (e.g. Donaldson 1982), spinifex textures in komatiites (Donaldson, 1982; Faure et al., 2006), dendritic olivines in oceanic picrites (Welsch, 2013) and ophiolitic dendritic chromite (Prichard et al., 2015). Hopper morphologies, reported here, represent a preserved intermediate stage of growth of chromite under moderately supercooled conditions.

Inclusions trapped in chromite

The 3D image of the inclusions in the chromite grains from Harold's Grave shows equant euhedral negative-crystal inclusions typical of those commonly described from ophiolite complexes. Some of these inclusions themselves (Fig. 6 B, D) have stepped surfaces. Such inclusions commonly contain several distinct silicate phases and are therefore distinct from accidental inclusions of pre-existing early-formed silicates such as olivine. Inclusions from the Harold's Grave samples are typically secondary assemblages of chlorite and serpentine, but in ophiolites as a whole inclusion mineralogy is widely variable and commonly includes alkali- and water-bearing phases such as phlogopite, sodic amphibole, quartz and alkali feldspar characteristic of advanced differentiation of silicate magma (e.g. Melcher et al., 1997; McElduff and Stumpfl, 1997). Several theories explain how negative crystal-shaped inclusions form, including entrapment of primary melt inclusions and sintering of multiple grains around pockets of trapped interstitial melt (Hulbert and Von Grunewald, 1985). We favour a process suggested by Vukmanovic et al. (2013) for "amoeboidal" chromite from the Merensky Reef of the Bushveld Complex, involving late-stage necking off the ends of deeply penetrating hopper pits by continuing growth of the enclosing grain. This process may occur at any stage between the accumulation temperature and the solidus; where it occurs close to the solidus, the inclusions trap highly evolved, residual silicate melt giving rise to the characteristic alkali-rich and water-rich inclusion assemblages. The close association between crystallographically aligned negative crystal inclusions and an immediately adjacent stepped hopper surface implies that the necking mechanism also applies to ophiolitic chromite (Fig. 8).

Formation of rounded chromite

The vast majority of the chromite crystals in ophiolitic massive and disseminated chromite are round or anhedral with smooth surfaces. A number of theories have been proposed to explain this. These include abrasion in a flowing magma in the tectonic environment of an oceanic spreading centre (Leblanc and Ceuleneer, 1992), deformation during magmatic crystallisation in a turbulent flowing magma (Stowe, 1994), resorption after incorporation of pre-existing faceted grains into transiently chromite undersaturated magma (Prichard et al., 2015) and sub-solidus annealing and sintering during postcumulus growth (Thayer, 1980) leading to adcumulate massive chromitite (Greenbaum, 1977).

We observed in the chromitites from ten different ophiolites (Fig. 7) that the shape of the chromite grains can be smooth with both concave and convex shapes where chromite is in contact with silicate, eliminating sintering of polycrystalline chromite aggregate as an explanation. We propose that the rounding of the chromite grains is caused by dissolution of the chromite in a chromite undersaturated magma producing convex chromite grain surfaces as has been suggested previously by Peters (1974). Leblanc (1980) observed pits or negative crystals with jagged boundaries on the smooth surfaces of chromite grains and he considered that these and the smooth surfaces were due to corrosion. We believe that these 'pits' are magmatic hopper growth structures that have been preserved and that the corrosion has destroyed the rest of the original magmatic growth of hoppers and euhedral chromitite to form smooth convex rounded surfaces. The hopper structures and equant cubic inclusions represent periods of chromite crystal growth whereas the rounded surfaces represent subsequent periods of dissolution and corrosion.

A model for ophiolitic chromite crystallisation

Our favoured model (Fig. 8) for ophiolitic podiform chromitites holds that they form during magma mixing or mingling or by the passage of sequential pulses of magmas (Arai and Yurimoto, 1994; Zhou et al., 1996; Paktunc, 1990; Ballhaus, 1998). These magmas have different compositions, from boninitic Cr-rich to MORB Cr-poor, whether formed by local melt rock reaction or input from magmas generated deeper in the mantle. Short-range variability in chromite and Os isotope composition within and between pods attest to this fluctuating magma supply (O'Driscoll et al., 2012; Derbyshire et al., 2013). We propose that the chromite pods grow by accretion at the margins of small, high-flux magma conduits, at high effective magma-crystal ratios necessary to permit the growth of chromite in the first place; chromite crystals represent concentration factors of many hundreds between 100-ppm levels in the magma and ~50% levels in the crystals (Murck and Campbell, 1986). The crystallising chromite grains are alternately bathed in variable composition magmas that will provide the varying degrees of supersaturation, for both crystal growth and corrosion. We propose that highly localised variations in nucleation rate, coupled with variable interactions with transiently undersaturated magma, give rise to the spectrum of chromite grain morphologies in ophiolites. High degrees of supercooling produce dendritic and hopper shaped chromite crystals; continuing growth of these grains under less supercooled conditions allows filling in spaces between dendrite arms or deeply penetrating hopper pits, resulting in the isolation of negative crystal inclusions. This produces scattered highly inclusion-rich sieve textured grains surrounded by inclusion-poor grains, a common observation exemplified in Fig 7L. Such associations represent mechanical mixtures of chromite grains with widely different thermal histories. Initially hopper textured grains may develop into euhedral grains with few inclusions where growth takes place in conditions of a steady supply of chromite saturated but not supercooled magma, in rare cases forming euhedral crystals of chromite such as those described by Leblanc and Ceuleneer (1992). More commonly, chromite grains are incorporated into flowing magma and either mechanically abraded or partially redissolved and corroded to give the common rounded shape of ophiolitic chromite (Fig. 8). The regime in which the chromite forms clearly varies from a chromite supersaturated, to a saturated and an undersaturated magma. This reflects the varying melt compositions that pass by or flow through the conduits where the chromite is crystallising..

Conclusions

These ophiolitic chromitites from Harold's Grave show a distinct chromite crystal morphology that may be characteristic of many ophiolitic chromitites. The surface morphology of this chromite shows euhedral crystal surfaces that include hopper crystal growth in 3D characteristic of formation in a chromite supersaturated magma. Examination of chromitites from 10 ophiolite complexes in 2D in polished thin sections reveals that these delicate hopper structures are commonly preserved. Composite polymineralic silicate inclusions in chromite grains formed by crystallisation of melt inclusions trapped by necking-off of concave cavities within the grains as the hopper crystals grew. Rounded chromite grains typical of crystal shape in ophiolite complexes may be produced as the end result of a sequence of processes. These include initial growth of chromite, possibly from a Cr-supersaturated boninite magma, to form hopper shaped crystals that subsequently fill in to form euhedral crystals. These are then corroded to form round shaped chromite grains in a chromite under saturated magma, possibly of MORB affinity. The hopper and corroded anhedral chromite textures are produced by variation in chromite saturation state in the magmas that pass through the mantle conduit where chromitite is crystallising.

Acknowledgements

Professor Hazel Prichard was working on this manuscript at the time of her death from a long illness in early January 2017. We acknowledge a Distinguished Visiting Fellowship for Prof. Prichard to CSIRO that made this work possible. Steve Barnes is funded by the CSIRO Science Leader scheme. We thank Brian O’Driscoll for his expeditious editorial handling, Mark Pearce (CSIRO for a helpful review of an early draft and two anonymous reviewers for constructive criticism.

Supplementary material

Fig S1. Animation of 3D scan of sample HG6A, approx. 1.2 mm diameter. All chromite surfaces shown in grey.

Fig. S2. Animation highlighting silicate melt inclusions (blue). Extrenal chromite grain surfaces removed for clarity. Image corresponds to Fig. 6.

Fig. S3. Animation highlighting pull-apart fracture surface and intersection with silicate inclusions inside chromite. External chromite grain boundaries removed for clarity.

Fig. S4. Animation of stepped chromite grain boundary, silicate inclusions removed for clarity. Box approx. 0.3 mm across.

References

Arai, S., and Yurimoto, H., 1994, Podiform chromitites of the Tari-Misaka ultramafic complex, Southwestern Japan, as mantle-melt interaction products: ECONOMIC GEOLOGY, v. 89, p. 1279-1288.

Ballhaus, C., 1998, Origin of podiform chromite deposits by magma mingling: Earth and Planetary Science Letters, v. 156, p. 185-193.

Barnes, S.J., 1986. The distribution of chromium among orthopyroxene, spinel and silicate liquid at atmospheric pressure. Geochimica et Cosmochimica Acta v. 50, 1889-1909.

Barnes, S.J., Jones, S., 2012, Deformed chromitite layers in the Coobina intrusion, Pilbara Craton, Western Australia: ECONOMIC GEOLOGY, v. 108, p. 337-354.

Barnes, S. J., Beresford, S. W., and Le Vaillant, M., 2016, Interspinifex Ni sulfide ore from the Coronet Shoot, Kambalda: characterisation using microbeam XRF mapping and 3D X-ray computed tomography: Economic Geology, v. 111, p. 1509-1517. doi:10.2113/econgeo.111.6.1509

Bridges, J.C., Prichard, H.M. and Meireles, C.A., 1995, Podiform chromitite-bearing ultramafic rocks from the Bragança Massif, northern Portugal: fragments of island arc mantle: Geological Magazine, v. 132, p.39-49.

Brough, C. P. Prichard, H. M**.** Neary, C. R. Fisher, P. C. and McDonald, I., 2015, Geochemical variations within podiform chromitite deposits in the Shetland Ophiolite: Implications for petrogenesis and PGE concentration: ECONOMIC GEOLOGY, v. 110, p. 187-208.

Brown, M., 1980, Textural and geochemical evidence for the origin of some chromite deposits in the Oman ophiolite, *in* Panayiotou, A., ed., Ophiloties Proceedings of the International ophiolite Symposium 1979, Cyprus: Nicosia, Cyprus Ministry of Agriculture and Natural Resources Geological Survey Department, p. 715-721.

Buades, A., Coll., B., and Morel, J.M., 2010, Image denoising methods: A new non-local principle: Siam review, p. 1–34.

Campbell, I. H., and Murck, B. W., 1993, Petrology of the G and H chromitite zones in the Mountain View area of the Stillwater Complex, Montana: Journal of Petrology, v. 34, p. 291-316.

Ceuleneer, G., and Nicolas, A., 1985, Structures in podiform chromite from the Maqsad district (Sumail ophiolite, Oman): Mineralium Deposita, v. 20, p. 177-185.

Derbyshire, E.J., O'Driscoll, B., Lenaz, D., Gertisser, R. and Kronz, A. (2013). Compositionally heterogeneous podiform chromitite in the Shetland ophiolite complex (Scotland); implications for chromitite petrogenesis and late stage alteration in the upper mantle portion of a supra-subduction zone ophiolite. Lithos (Oslo), 162-163, 279-300.

Donaldson, C.H., 1982, Origin of some Rhum harrisite by segregation of intercumulus liquid: Mineralogical Magazine, v. 45, p. 201-209.

Dowling, S.E., Barnes, S.J., Hill, R.E.T., and Hicks, J.D., 2004, Komatiites and nickel sulfide ores of the Black Swan area, Yilgarn Craton, Western Australia. 2: geology and genesis of the orebodies: Mineralium Deposita ,v. 39, p. 707–728.

Faure, F., Arndt, N. T., and Libourel, G., 2006, Formation of spinifex textures in komatiites: an experimental study: Journal of Petrology, v. 47, p. 1591-1610.

Flinn, D., 1985, The Caledonides of Shetland, *in* Gee., D.G.and Sturt., B. A., eds., The Caledonide Orogeny - Scandinavia and related Areas: John Wiley and Sons Ltd., p. 1159-1172.

Godel, et al., 2010, Platinum ore in 3D: Insights from high-resolution X-ray computed tomography.: Geology, v. 38, p. 1127−1130.

Godel, B. 2013, High resolution X-ray computed tomography and its application to ore deposits: case studies from Ni-Cu-PGE deposits: ECONOMIC GEOLOGY, v. 108, p. 2005-2019.

Godel, B., 2015, Platinum-Group Element Deposits in Layered Intrusions: Recent Advances in the Understanding of the Ore Forming Processes, *in* Charlier, B., Namur, O., Latypov, R., Tegner, C. eds., Layered Intrusions: Springer Netherlands, p. 379-432.

Godel, B., Barnes, S.J., Gürer, D., Austin, P., and Fiorentini, M.L., 2013, Chromite in komatiites: 3D morphologies with implications for crystallization mechanisms: Contributions to Mineralogy and Petrology, v. 165, p. 173-189.

Hounsfield, 1973, Computerized transverse axial scanning tomography. 1. Description of system. British Journal of Radiology 46, 1016–1022.

Greenbaum, D., 1977, The chromitiferous rocks of the Troodos ophiolite complex, Cyprus : ECONOMIC GEOLOGY, v. 72, p. 1175-1194.

Hulbert, L.J., and Von Gruenewaldt, G., 1985, Textural and compositional features of chromite in the lower and critical zones of the Bushveld complex South of Potgietersrus: Economic Geology, v. 80, p. 872–895.

Jerram, D.A., Davis, G.R., Mock, A., Charrier, A. and Marsh, B.D. (2010) Quantifying 3d crystal populations, packing and layering in shallow intrusions; a case study from the basement sill, dry valleys, antarctica. Geosphere, 6, 537-548.

Ketcham, R. A. & Carlson, W. D. (2001). Acquisition, optimization and interpretation of X-ray computed tomographic imagery: applications to the geosciences. Computers & Geosciences 27, 381–400.

Kozul, H., Prichard, H.M., Melcher, F., Fisher, P.C., Brough, C., and Stueben, D., 2014, Platinum-group element (PGE) mineralisation and chromite geochemistry in the Berit ophiolite (Elbistan/Kahramanmaraş), SE Turkey: Ore Geology Reviews, v. 60, p. 97-111.

Leblanc, M., 1980, Chromite Growth, Dissolution and Deformation from a Morphological View Point: SEM Investigations: Mineralium Deposita, v.15, p. 201-210.

Leblanc, M., and Ceuleneer, G., 1992, Chromite crystallization in a multicellular magma flow:Evidence from a chromitite dike in the Oman ophiolite: Lithos, v. 27, p. 231-257.

McElduff, B., and Stumpfl, E.F., 1991, The chromite deposits of the Troodos Complex, Cyprus-evidence for the role of a fluid phase accompanying chromite formation: Mineralium Deposita, v. 26, p. 307-318.

Melcher, F., Grum, W., Simon, G., Thalhammer, T.V., and Stumpfl, E. F., 1997, Petrogenesis of the ophiolitic giant chromite deposits of Kempirsai, Kazakhstan: a study of solid and fluid inclusions in chromite: Journal of Petrol, v. 38, p. 1419-1458.

Murck, B. W., and Campbell, I. H., 1986, The effects of temperature, oxygen fugacity and melt composition on the behaviour of chromium in basic and ultrabasic melts: Geochimica Cosmochimica Acta, v. 50, p. 1871-1888

O'Driscoll, B., Emeleus, C.H., Donaldson, C.H., Daly, J.S., 2010, Cr-spinel seam petrogenesis in the Rum layered suite, NW Scotland: cumulate assimilation and in situ crystallisation in a deforming crystal mush: Journal of Petrology, v. 51, p. 1171-1201.

O'Driscoll, B., Day, J.M.D., Walker, R.J., Daly, J.S., McDonough, W.F. and Piccoli, P.M. (2012) Chemical heterogeneity in the upper mantle recorded by peridotites and chromitites from the shetland ophiolite complex, scotland. Earth and Planetary Science Letters, 333-334, 226-237.

Pagé, P., and Barnes, S.J., 2009, Using trace elements in chromites to constrain the origin of podiform chromitites in the Thetford Mines ophiolite, Quebec, Canada: Economic Geology, v. 104, p. 997-1018.

Paktunc, A,D., 1990, Origin of podiform chromite deposits by multistage melting, melt segregation and magma mixing in the upper mantle: Ore Geology Reviews, v. 5, p. 211-222.

Pedersen, R.B., Johannesen, G.M., and Boyd, R., 1993, Stratiform PGE mineralisations in the ultramafic cumulates of the Leka ophiolite complex, central Norway: Economic Geology, v. 88, p. 782-803

Peters, T.J., 1974, Chromite Deposits in the Ophiolite Complex of Northern Oman: Mineralium Deposita, v. 9, p. 253-259.

Philpotts, A.R. and Dickson, L.D. (2000) The formation of plagioclase chains during convective transfer in basaltic magma. Nature, 406, 59- 61

Prichard, H.M., 1985, The Shetland Ophiolite, *in* Gee, D.G., and Sturt, B.A., eds., The Caledonide Orogen: Scandinavia and related area, Volume 2: Wiley and Sons Ltd. , p. 1173-1184.

Prichard, H.M., and Neary, C.R., 1981, Chromite in the Shetland Islands ophiolite complex, *in* An International Symposium on Metallogeny of Mafic and Ultramafic complexes: Athens UNESCO Project 169, v. 3, p. 343-360.

Prichard, H.M., and Lord, R.A., 1988, The Shetland ophiolite: Evidence for a supra-subduction zone origin and implications for PGE mineralisation, *in* Boissonnas, J. and Omenetto, P., eds., Mineral Deposits in the European Community: Springer Verlag, p. 289-302.

Prichard, H.M., Potts, P.J., Neary, C.R., Lord, R.A., and Ward, G.R., 1989, Development of techniques for the determination of the platinum-group elements in ultramafic rock complexes of potential economic significance: mineralogical studies, Luxembourg, Commission of the European Communities, 170pp.

Prichard, H.M., Neary, C.R., Fisher, P.C., and O'Hara, M.J., 2008a, PGE-rich podiform chromitites in the Al'Ays Ophiolite complex, Saudi Arabia: An example of critical mantle melting to extract and concentrate PGE: ECONOMIC GEOLOGY, v. 103, p. 1507-1529.

Prichard, H.M., Economou-Eliopoulos, M., and Fisher, P.C., 2008b, Platinum-group minerals in podiform chromitite in the Pindos ophiolite complex, Greece: Canadian Mineralogist, v. 46, p. 329-341.

Prichard, H.M., Barnes, S. J., Godel, B., Halfpenny, A., Neary, C.R., and Fisher, P.C., 2015, The structure of and origin of nodular chromite from the Troodos ophiolite, Cyprus, revealed using high-resolution X-ray computed tomography and electron backscatter diffraction: Lithos, v. 218-219, p. 87-98.

Roberts, S., and Neary, C.R., 1993, Petrogenesis of ophiolitic chromitite, *in* Prichard, H.M., Alabaster, T., Harris, N.B., and Neary, C.R., eds., Magmatic Processe sand Plate Tectonics, Volume 76: Geological Society Special Publication, p. 257-272.

Stowe, C.W., 1994, Compositions and tectonic settings of chromite deposits through time: ECONOMIC GEOLOGY, v. 89, p. 528-546.

Thayer, T.P., 1980, Syn-crystallization and subsolidus deformation in ophiolitic peridotite and gabbro: American Journal of Science, v. 280-A, p. 269-283.

Vukmanovic,Z., Barnes, S.J., Reddy, S.M., Godel, B., and Fiorentini, M.L., 2013, Morphology and microstructure of chromite crystals in chromitites from the Merensky Reef (Bushveld Complex, South Africa): Contributions to Mineralogy and Petrology, v. 165, p. 1031-1050.

Welsch, B., Faure, F., Famin, V., Baronnet, A. and Bachelery, P. (2013) Dendritic crystallization; a single process for all the textures of olivine in basalts? Journal of Petrology, 54, 539-574.

Yang, K., and Seccombe, P. K., 1993, Platinum-group Minerals in the Chromitites from the Great Serpentinite Belt, NSW, Australia: Mineralogy and Petrology, v. 47, p. 263-286.

Zhou, M.-F., Robinson, P.T., Malpas, J., and Li, Z., 1996, Podiform Chromitites in the Luobusa Ophiolite (Southern Tibet): Implications for Melt-Rock Interaction and Chromite Segregation in the Upper Mantle: Journal of Petrology, v. 37, p. 3-21.

Prichard et al Min Mag Figure Captions

Figure 1. Photomicrographs illustrating the difference in shape between ophiolitic (A and B) and layered complex (C and D) chromite grains. A) Al 'Ays, Saudi Arabia B) Semail, Oman, C) Bushveld, RSA and D) Stillwater, USA.

Figure 2. Map of the Shetland ophiolite and Harold's Grave locality (diagram from Brough et al. 2014).

Figure 3. Examples showing details of the reconstructed virtual core (scanned at 700 nm voxel size) within a 4 mm diameter core drilled through a larger specimen (HG6A described in Brough et al. (2015)) of chromitite from the Harold's Grave. A) Volume rendering of the virtual core showing the 3D distribution of chromite (lighter grey) and silicates and the orientation of slices along the XY (B) , YZ (C) and XZ (D) planes. A, B and C) 2D slices virtually cut through the core along the 3-planes and show chromite (grey with lighter colour due to secondary Fe-enrichment along fine fractures) and silicates (dark grey to black). The white arrows show areas of stepped edges of the chromite crystals; 1 – shows the intersection of negative crystal silicate inclusions in the chromite; 2 – shows secondary pull apart structures cross-cutting crystal negative silicate inclusions in the chromite; 3 – shows pull-apart structures cross-cutting the entire chromite crystal. PGM: platinum-group mineral.

Figure 4. 3D isosurfaces showing the 3D textures of chromite crystal from chromitite from Harold's Grave. A) Image showing the internal structures of the chromite crystal with silicate inclusions; B) Image showing the internal structure of the chromite crystal where silicate inclusions have virtually been removed; C) Image showing the surface of chromite where the depression represents the centre of a hopper crystal; D) Image showing the details of the smooth surface of secondary pull-apart structures that in some cases cross-cut negative crystal silicate inclusions; note marked contrast between this fracture surface and the primary stepped crystal face; and E) Image showing in 3D the stepped surface of the chromite crystal. See supplementary s3 and s4 for animated versions.

Figure 5. A) Diagram of an ideal chromite hopper crystal showing cross section planes represented by dashed lines (S1 and S2). B) 2D cross-section along the plane S1 showing a stepped depression in the surface of the chromite that may be filled with interstitial silicates and C) 2D cross-section along the plane S2 (i.e. at right angle to S1) showing a thin rim of chromite around or enclosing space that is also likely to be filled with silicates.

Figure 6. 3D isosurfaces showing the 3D textures of chromite crystal and the distribution of the negative crystal silicate inclusions observed in the chromitite from Harold's Grave. A) and B) Images showing the internal structures of the chromite crystal where negative crystal silicate inclusions (blue) are located within planes parallel to the chromite surface (in grey); c) Image showing the distribution of the entire silicates inclusion population observed within the entire chromitite micro-core and D) Images showing details of the 3D structures of the largest silicate inclusion observed in the micro-core and rotated along the black arrow. See supplementary S1 and S2 for animations.

Figure 7. Photomicrographs of chromite grains (pale grey) with hopper edges and silicate inclusions in chromitites from ophiolite complexes. A) and B) Shetland ophiolite A) Harold's Grave, C) Bragança, Portugal, the hollow square of chromite may be a plan view of a hopper crystal (See Fig. 2C S2) and a similar hollow square of chromite is partially incorporated into the main chromite, D) Al 'Ays. Saudi Arabia, E) Leka, Norway F) Limassol Forest, Troodos, Cyprus, G) Kempersai Kazakhstan, H) Santa Elena, Costa Rica, I) Berit, Turkey, J) Semail, UAE, showing a transition from a smooth convex chromite grain (bottom left) to stepped chromite edges (top right), K) and L) Pindos Greece, L)

shows inclusions in only one chromite grain, M) Semail, UAE, abundant silicate inclusions extend into the chromite grain away from the stepped edge.

Figure 8. A model for the growth of chromite crystals. A) a skeletal crystal forms which is a hopper crystal when viewed in 3D, B) infilling in 3D allows the skeletal crystal to form a hopper crystal on the surface and traps melt inclusions, C) abundant Cr supply allows hopper crystals to infill and an euhedral chromite crystal forms and D) the chromite crystal is then corroded to give the characteristic typical shape of individual chromite crystals in ophiolitic chromite.

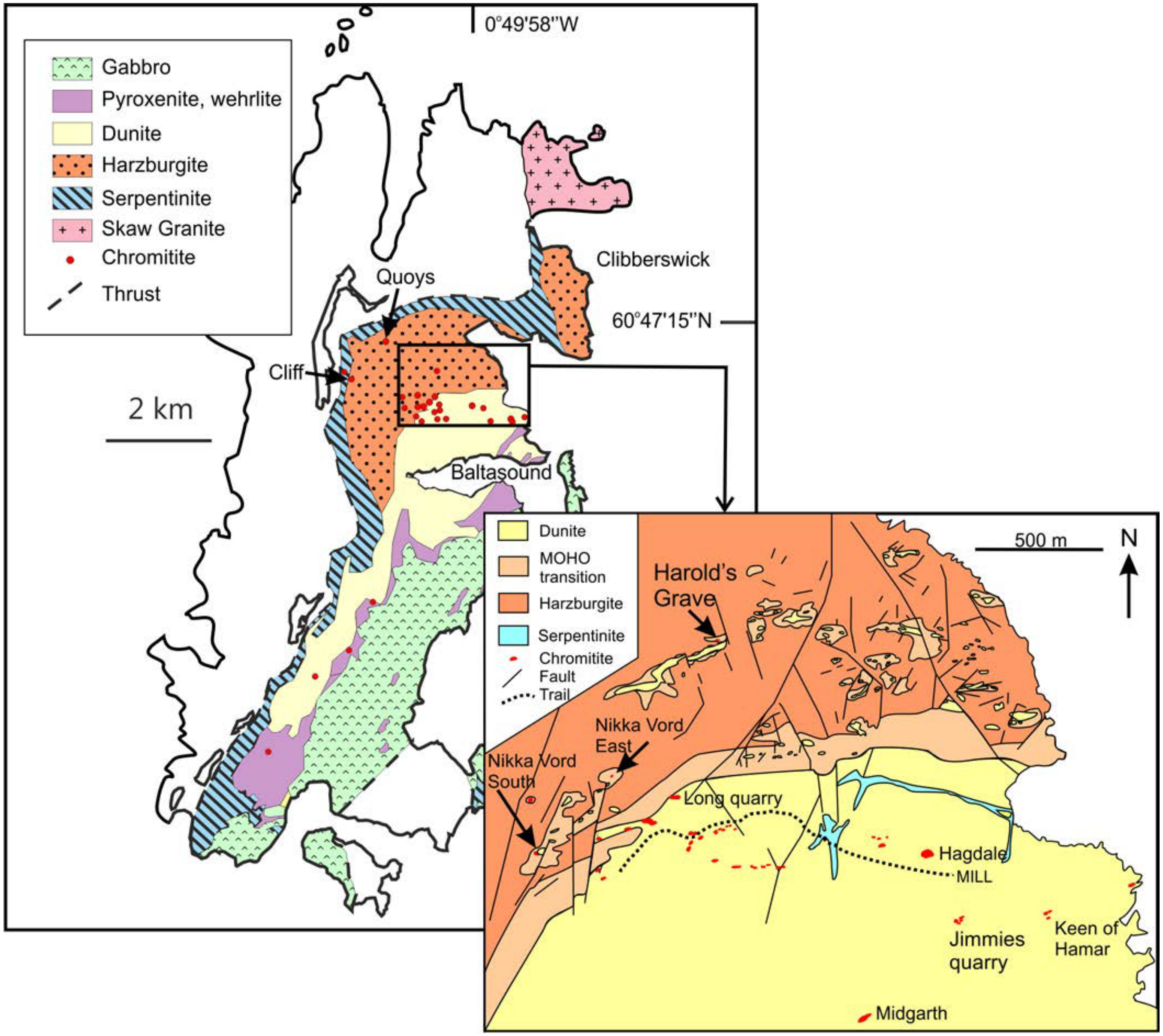
Gabbro
Pyroxenite, wehrlite
Dunite
Harzburgite
Serpentinite
Skaw Granite
Chromitite
Thrust
0°49'58''W
60°47'15''N
Clibberswick
Quoys
Cliff
2 km
Baltasound
Dunite
MOHO transition
Harzburgite
Serpentinite
Chromitite
Fault
Trail
500 m
N
Harold's Grave
Nikka Vord East
Nikka Vord South
Long quarry
Hagdale
MILL
Keen of Hamar
Jimmies quarry
Midgarth

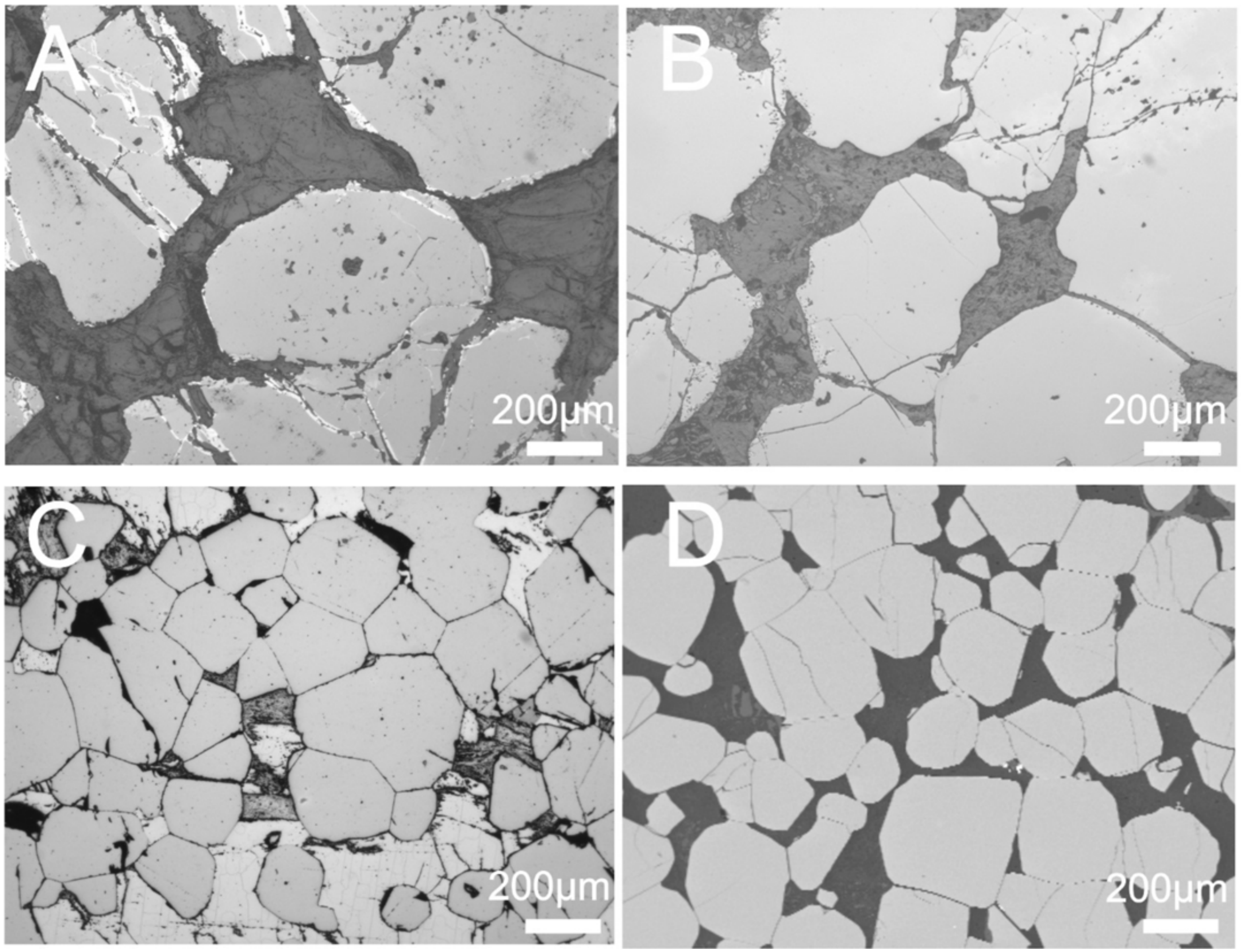
A
200µm
B
200µm
C
200µm
D
200µm

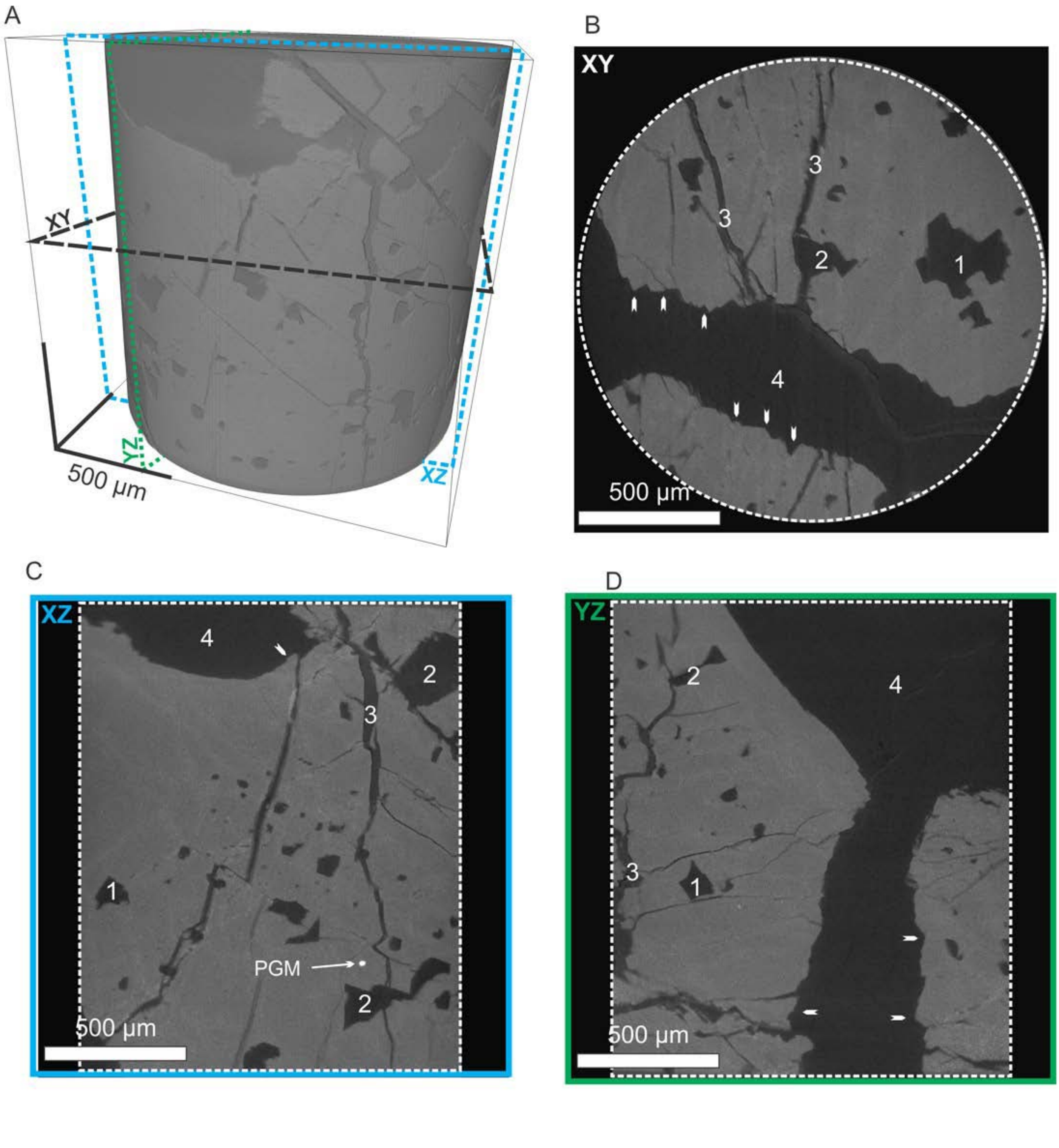
A
XY
YZ
500 µm
XZ
B
XY
3
3
2
1
4
500 µm
C
XZ
4
2
3
1
PGM
2
500 µm
D
YZ
2
4
3
1
500 µm

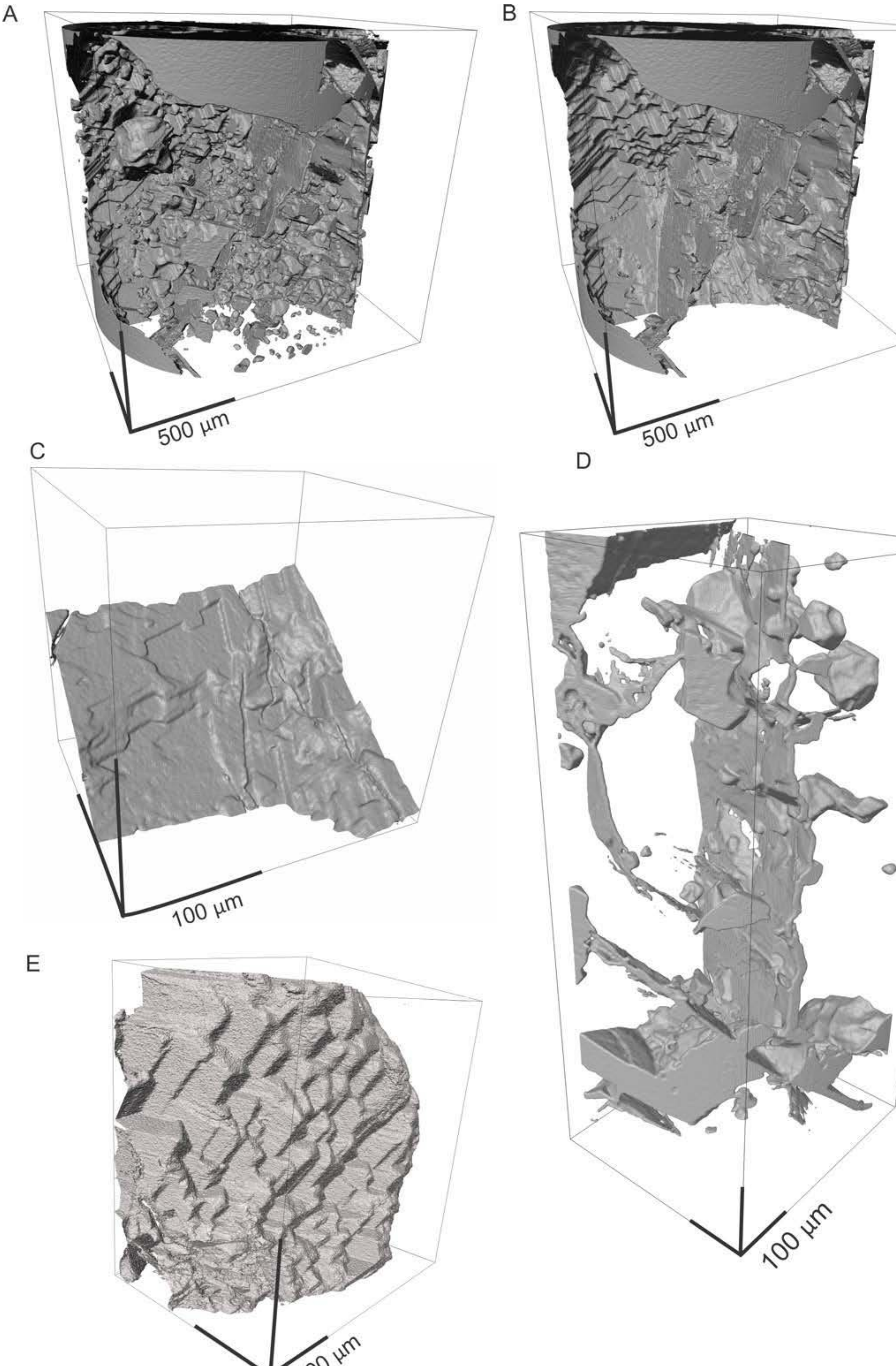
A
500 µm
B
500 µm
C
100 µm
D
100 µm
E
100 µm

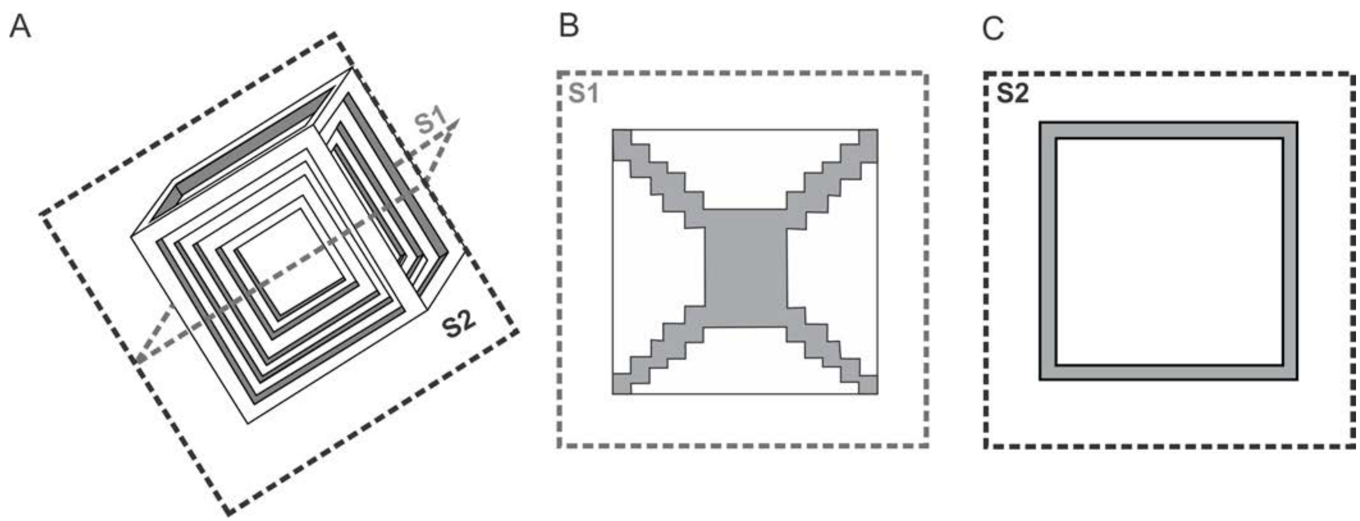
A
S1
S2
B
S1
C
S2

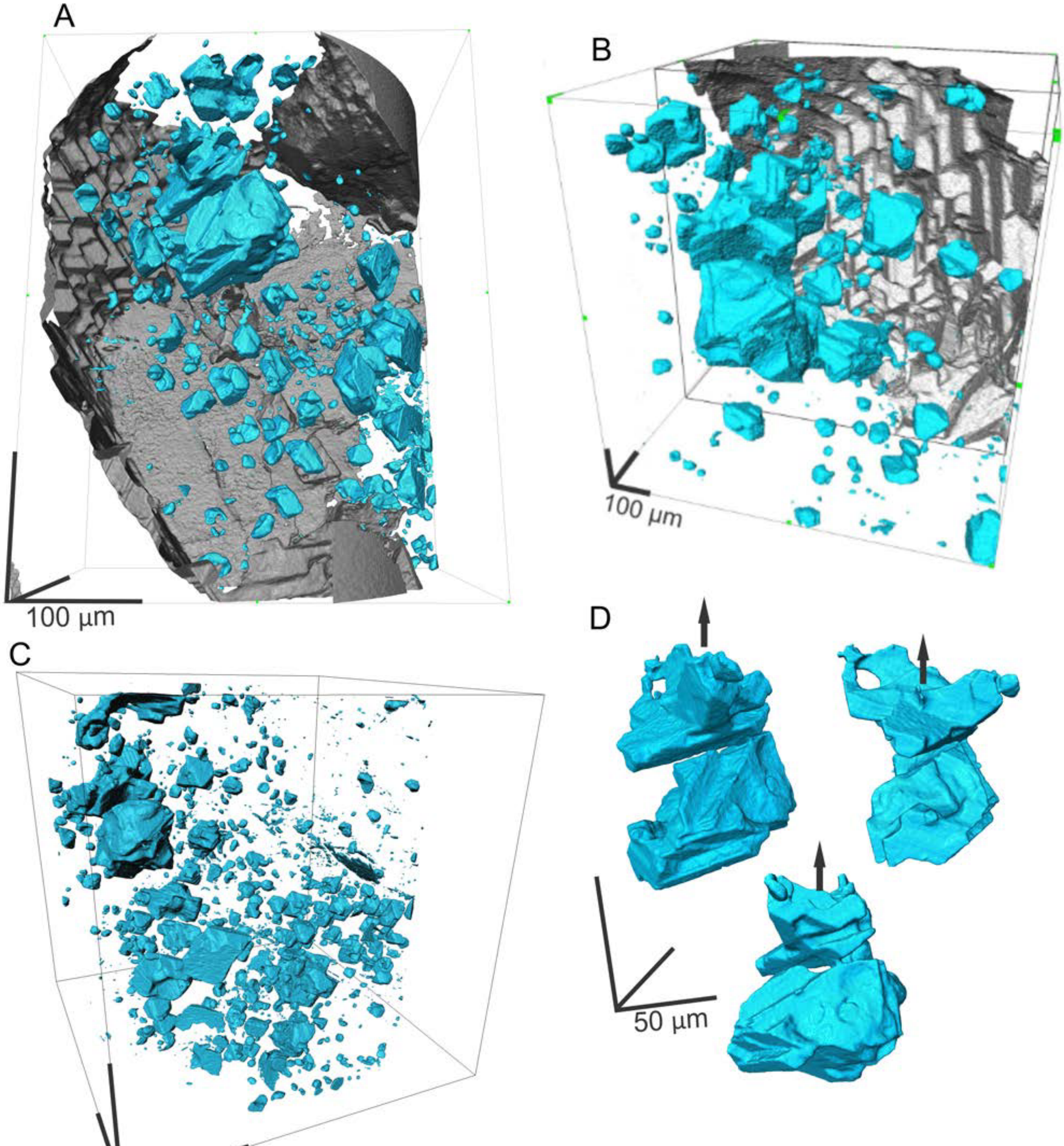
A
B
100 µm
100 µm
C
D
50 µm
500 µm

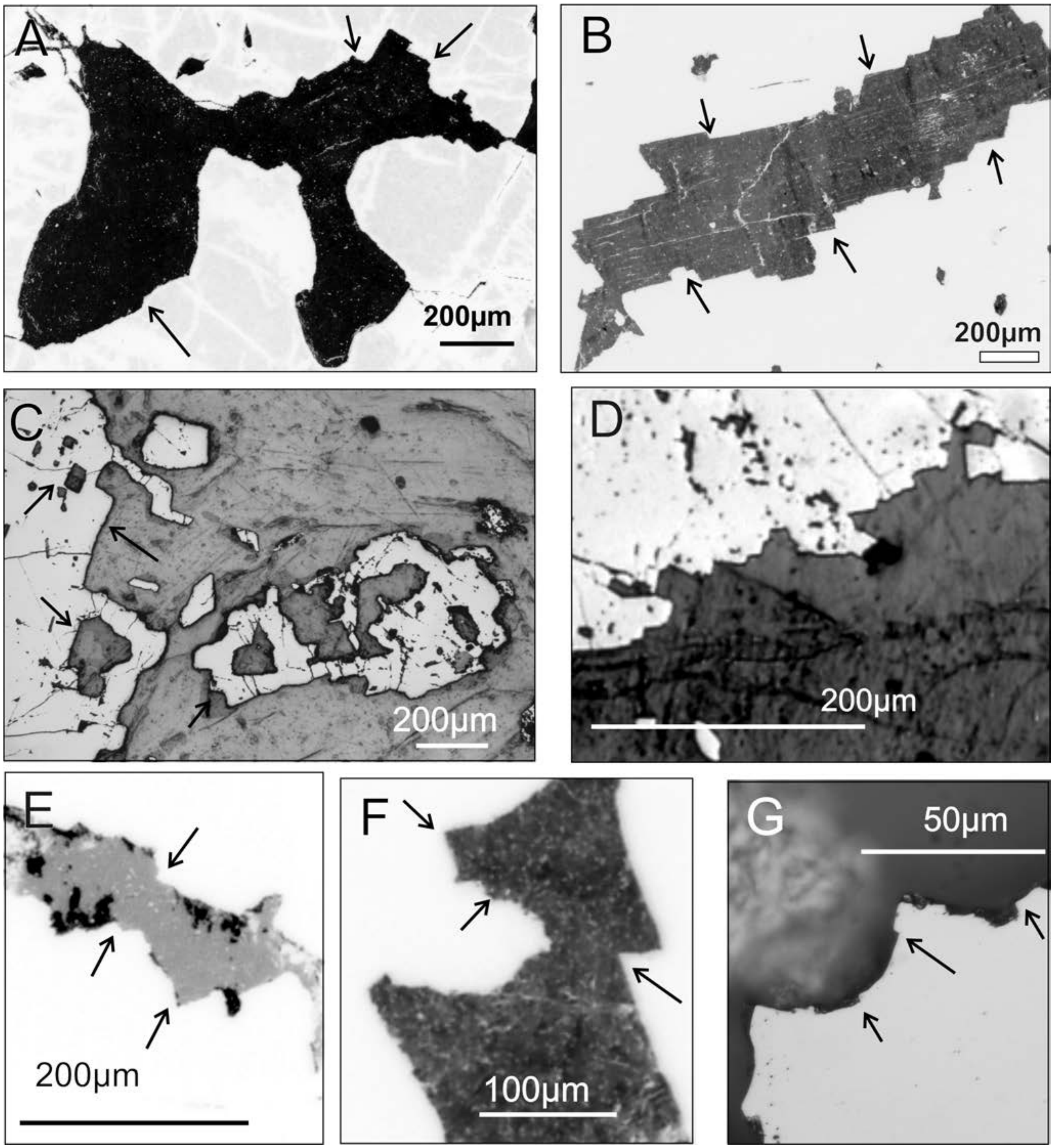
A
200µm
B
200µm
C
200µm
D
200µm
E
200µm
F
100µm
G
50µm

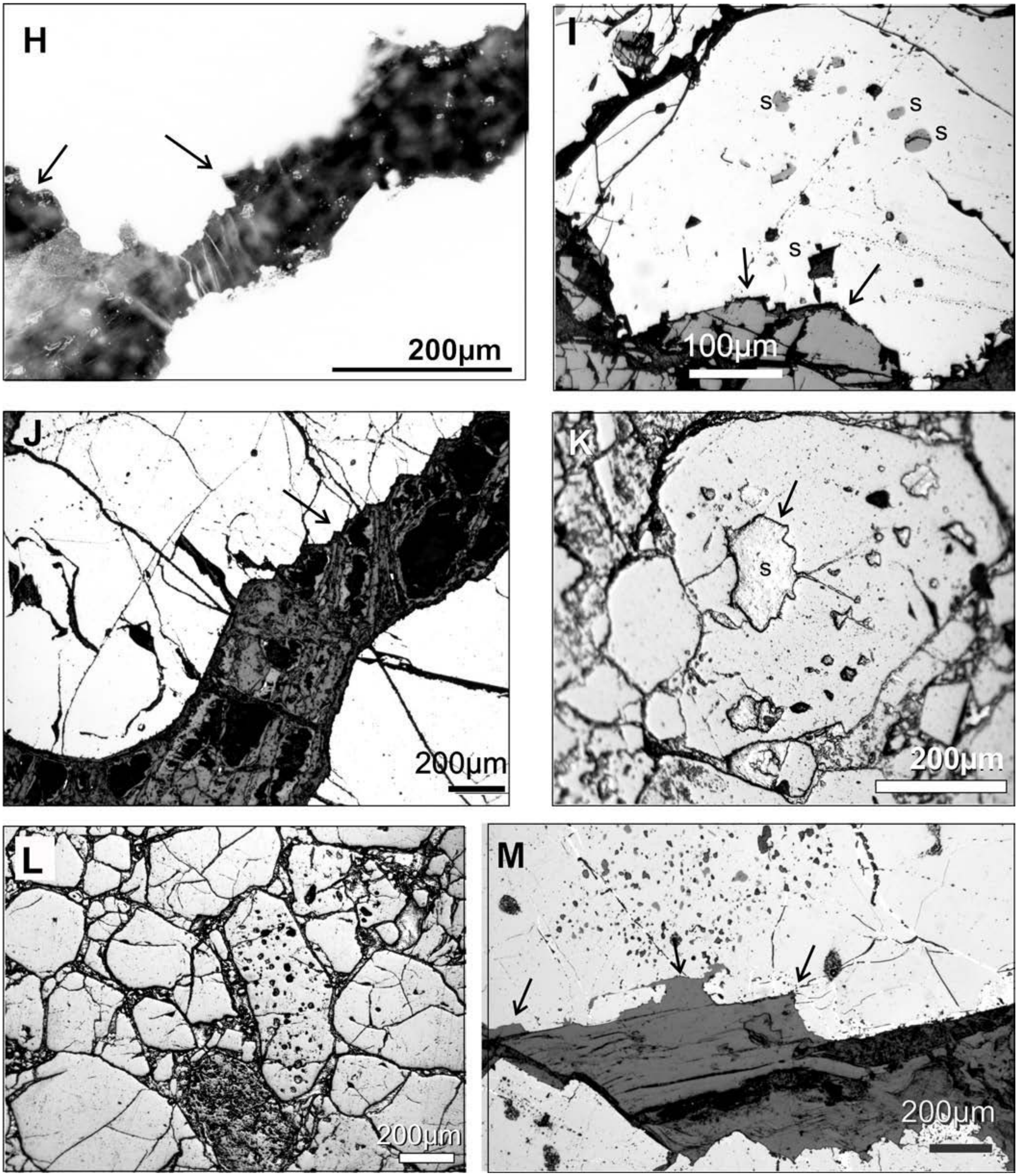
H
200µm
I
s
s
s
s
100µm
J
200µm
K
s
200µm
L
200µm
M
200µm

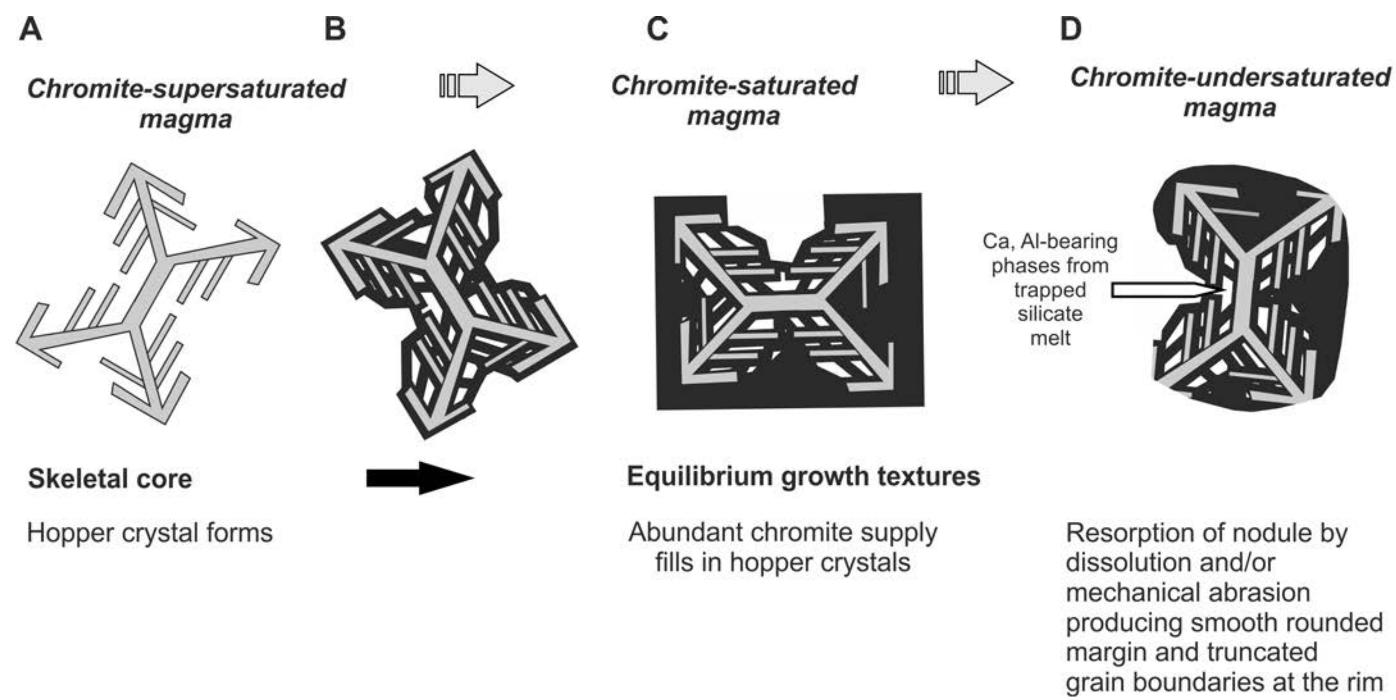
A
B
C
D
Chromite-supersaturated magma
Chromite-saturated magma
Chromite-undersaturated magma
Ca, Al-bearing phases from trapped silicate melt
Skeletal core
Hopper crystal forms
Equilibrium growth textures
Abundant chromite supply fills in hopper crystals
Resorption of nodule by dissolution and/or mechanical abrasion producing smooth rounded margin and truncated grain boundaries at the rim

Ophiolite	Age	Type, parent magmas	Reference to chromitite
Al ‘Ays, Saudi Arabia	Eocambrian	Back-arc	Prichard et al., 2008a
Berit, Turkey	Late Cretaceous	Oceanic arc	Kozlu et al., 2014
Bragança, Portugal	Devonian	Supra-subduction, Island arc picrite	Bridges et al., 1995
Kempersai, Khazakhstan	Early Devonian	Ocean floor to arc; MORB lavas	Melcher et al., 1997
Leka, Norway	Cambrian (Caledonian orogeny)	Supra-subduction, Island arc tholeiite to MORB	Pedersen et al., 1993
Pindos, Greece	Eocene	Supra-subduction, MORB to island arc tholeiite.	Prichard et al., 2008b
Santa Elena, Costa Rica	Early Cretaceous	Plume type, P-MORB	Prichard et al., 1989
Semail, Oman	Late Cretaceous	Fore-arc: MORB, IAT, boninite	Brown, 1980
Shetland	Late Cambrian (Caledonian orogeny)	Supra-subduction, MORB plus boninite	Prichard and Lord 1988
Troodos, Cyprus	Late Cretaceous	Fore-arc: MORB, IAT, boninite	McElduff and Stumpfl, 1991